Estimation of the Noise Contributions from Blank, Transmission and Emission Scans in PET

Søren Holm†, Peter Toft‡, and Mikael Jensen†
† Dept. of Nuclear Medicine, Rigshospitalet, National University Hospital, Copenhagen, Denmark (sholm@pet.rh.dk).
‡Electronics Institute, Technical University of Denmark (ptoft@ei.dtu.dk).

Abstract

This work determines the relative importance of noise from blank (B), transmission (T) and emission (E) scans in PET using a GE Advance scanner on a 20 cm cylinder, a brain phantom, and a torso-like ellipse (18/35 cm) with examples of human scans (brain O-15 water and F-18 FDG, heart FDG). Phantom E scans were acquired in both 2D and 3D modes as decay series with C-11 or F-18 over 3-6 decades of Noise Equivalent Counts (NEC). B and T scans were made using two pin sources (389+134 MBq) with times 16-32768 sec. In humans only a limited subset was available. In homogeneous phantoms normalized variance (var) was estimated from pixel distributions in single images. In other objects, including the human studies, calulations were performed on differences of paired images. In all cases a fit was made to a simple noise model. The cylinder data shows expected relations of T to B noise proving the adequacy of B scan times < 30 min for most purposes. For cylinder and brain phantom, contour plots are provided for var(E,T). In a typical 3D O-15 water study with 0.5M counts per central slice, a 10 min T-scan ensures that var(T)<0.1*var(E). Using 10 min T scan for a static 3D FDG brain study of 10 min having 5M counts yields equal E and T variance contributions. In human body scans T noise has a relative larger importance and is often dominated by effects of line artefacts from (clusters of) zeros in the T-scan, not included in the simple model.

I. Introduction

The purpose of this work is to establish guidelines for the relative importance of the noise contributions from blank, transmission and emission scans in typical imaging situations in PET. Although much information can be deduced theoretically from existing knowledge of reconstruction algorithms [1, 2], we have mainly applied an experimental approach. The limitations in generality caused by the obvious difficulty of varying all of the many possible parameters of acquisition and reconstruction are outweighed by the advantage of the close reproduction of actual scan setups, and direct testing in some human studies. The following paragraph describes the model used for fitting to the observed data.

II. Theory

Due to the the linearity of the reconstruction process the PET images (volumes) x_i, can be described as a weighted sum of the sinogram values s_j, with weight factors ϕ_{ij} corresponding to the actual (linear) reconstruction algorithm

$$x_i = \sum_j \phi_{ij} s_j \tag{1}$$

where the actual image pixel (voxel) is denoted by i, and j denotes the pixel position in the sinogram. In order to compensate for attenuation the sinogram used for reconstruction is calculated from an emission sinogram e_j, a transmission sinogram t_j, and a blank scan b_j. The calculation basically amounts to:

$$s_j = \frac{e_j b_j}{t_j} \tag{2}$$

although this is usually qualified by a filtering of the factor $\frac{b_j}{t_j}$.

All three types of sinograms in principle inherit their statistical properties from the Poisson statistics of the radioactive decay. A number of corrections that are performed before the stage of reconstruction described here, however, adds to the raw counts' noise. The overall effect of correction for randoms and scatter can be described as a decrease in effective counts [3], the resulting figure being widely known as Noise Equivalent Counts (NEC). A practical formulation used in this work is:

$$NEC = T\frac{(1-SF)^2}{1+2f\frac{R}{T}} \tag{3}$$

where T is true counts (including scatter), R is random counts from the full field-of-view, f is the fraction of the sinogram covered by the object under investigation, and SF is the scatter fraction. In all applications of NEC in this study, the value of SF has been set to zero. Within this paper NEC per slice is used as a parameter.

A. *The Noise Model*

In the simplest case where the image noise is estimated from a single image set, using a Taylor expansion and disregarding noise correlation between pixels implies that the pixel noise variance $V\{x_i\}$ can be estimated by

$$V\{x_i\} \simeq \sum_j \phi_{ij}^2 V\left\{\frac{e_j b_j}{t_j}\right\}$$
$$\simeq \sum_j \phi_{ij}^2 E^2\{s_j\}\left[\frac{V\{e_j\}}{E^2\{e_j\}}+\frac{V\{b_j\}}{E^2\{b_j\}}+\frac{V\{t_j\}}{E^2\{t_j\}}\right] \quad (4)$$

Due to the Poisson statistics the variance in the emission sinogram relative to the squared mean value $\frac{V\{e_j\}}{E^2\{e_j\}}$ is inversely proportional to the mean $E\{e_j\}$, i.e., inversely proportional to number of counts NEC in the emission sinogram. Similar arguments can be used for the transmission and blank scan terms, hence the total pixel variance normalized with the mean of the image can be modelled by

$$\frac{V\{x_i\}}{E^2\{x_i\}} = \frac{a}{NEC} + b + \frac{c}{T_t} + \frac{d}{T_b} \quad (5)$$

where T_t is the transmission scan time in seconds, T_b the blank scan time in seconds (for the given geometry and source strength). In the model a base term b is included to accommodate effects in the reconstruction process, not explained by the other terms, e.g., varying sensitivity of the detectors, not properly corrected for by normalization.

In this paper all measured data have been fitted to the model shown in Equation 5. In cases with heterogeneous ROI's the variance was measured for differences between equivalent and independent images [6]. In these cases the measured normalized variance has been divided by two so estimated noise parameters are directly comparable.

III. Methods

Measurements were made on the GE Advance scanner [8, 9] with 3D acquisition and reconstruction capability. Its 9 GByte raw data disk can hold about 180 3D frames (byte mode, separate prompts and delayed), convenient for phantom decay studies. Reconstruction in our configuration takes approximately 8 minutes per frame. The scanner applies two pin sources for blank and transmission scanning. During the initial experiments the pin source activities were 389 MBq and 134 MBq, respectively, and the blank scan sinogram count rate was 0.91 Mcps. On later phantom and human studies, blank and transmission scan times have been scaled in accordance with the currently observed blank scan count rates and the values quoted in seconds (powers of 2) are therefore assumed to be directly comparable.

A. *Phantom studies*

Three different water-filled phantoms have been used: the 20 cm standard (NEMA) cylinder, a torso-like ellipse with axes 18 and 35 cm, and an axially symmetrical, elliptical brain phantom (Capintec) with axes 15 and 20 cm.

Using initially the two homogeneous phantoms in accordance with Equation 5, emission scans were made in both 2D and 3D as decay series with F-18 starting at rates well below saturation of the scanner. In 2D a total of 22 measurements were performed starting with a half-life of F-18 and then reducing the time down to ...,4,2,1 seconds, effectively reducing the number of counts by a factor of 2 for each acquisition. In 3D the dataset was limited to 10 time frames. Transmission scans were made starting from T_t=16 seconds (64 on the ellipse) and doubling the time for each step up to 32768 seconds. Blank scans were made from T_b=16 to 4096 seconds and complemented with one 100000 seconds scan.

Reconstructions were made for all relevant combinations of emission and transmission scans using the 2048 seconds blank scan. All emission scans were further reconstructed with a calculated attenuation correction (CAC) using a circular or elliptical contour respectively. For the 2D cylinder case the emission image with highest count was reconstructed with the longest transmission scan and all blank scans. The cylinder was reconstructed in a 128^2 matrix with pixel size 2.0 mm, and a Hann filter (designated '4 mm' corresponding to the approximate resulting resolution FWHM). For the ellipse, a 128^2 matrix of pixel size 4.0 mm was used with a Hann '8 mm' filter. The 3D reconstruction further contains an axial filtering (Hann) set to its minimum value of 8.5 mm. The attenuation data were preprocessed with a Gaussian filter, 8 mm for the cylinder case, and 10 mm for the ellipse. All available corrections were applied, including detector normalization, randoms subtraction, scatter correction, (slice) sensitivity and absolute calibration, and decay correction to scan start. In all slices of all reconstructed images (order of 25,000 images) the mean and variance was calculated from an ROI extending 70% of the diameter or ellipse axes. These ROI-data were imported to MATLAB for further analysis. In 2D the data were averaged over 31 (of 35) slices avoiding edge effects but ignoring the minor differences between direct and cross slices. In 3D only the central 15 slices having almost identical noise were included in the average. For each reconstructed dataset the noise was represented by the normalized variance, i.e., variance/mean^2, in subsequent plots and fitting. From the total rates curves acquired with the images a Noise Equivalent Count (NEC) value per slice was calculated for each scan frame. The rate dependent correction between trues and NECs due to randoms was in all these cases below 15% except in the first 3D cylinder frame where it amounted to 25%.

The brain phantom has two separate chambers ('grey' and 'white' matter, respectively). It was filled to resemble the usually quoted ratio of 4:1 between these two substances for flow or metabolism. During scanning the phantom was embedded in a Rando-Alderson whole body phantom (normally used for radiotherapy dosimetry purposes) from which a few slices of the head had been removed. Also the thorax was replaced by the body ellipse phantom containing 5 times the total activity in the brain to provide more natural scatter and randoms conditions than the brain phantom alone. Two different sets of measurements have been performed. One set (repeated in 2D and 3D) was originally designed to address count rate performance [4]. The phantoms were loaded with C-11 Carbonate well above the expected saturation limit of the scanner and pairs of (60:62) seconds scans were performed every 10 minutes for about 5 hours (15 half lives). The relatively short half life of C-11 and the intention of having not only similar counts but also count rates in each of the two paired scans limited the maximum number of slice counts observed to 10^6 which would not allow a sufficiently clear distinction between the transmission scan times. One more decay series therefore was prepared in 3D with F-18 starting below maximum counts, and measuring for 12 half lives utilizing all the time for recording. Each of the half lives were split in two frames with a ratio of (0.415:0.585) yielding approximately equal counts. The C-11 series were reconstructed using an 'infinite' (32768 second) transmission scan. For the F-18 series, a set of 7 pairs of transmission scans were obtained (32,64,128,256,1024,4096,16384) seconds. Reconstructions were made to provide datasets with independent transmission and emission noise by combining the E-T frames as odd-odd, even-even. Reconstruction parameters for the brain phantom were identical to those for the cylinder except that the axial Hann filter was here replaced by a ramp filter. From both the C-11 series and the F-18 series, difference images were calculated, whole brain ROI's were placed in the original as well as the difference images for mean and standard deviation calculation respectively.

B. *Human studies*

For one person (case KL) included in a count rate performance and dose optimization study with O-15 [4] the usual 90 second integration time (starting 20 seconds after bolus injection) was supplemented by 2 short frames (20-22 seconds). The study comprised injections with 25-800 MBq in 2D and 50-800 MBq in 3D. Reconstruction and analysis was performed as above, although only with one 12 minutes transmission scan. The number of NECs in the short scans were about 16% of the corresponding 90 seconds frames normally used.

One person (case MN) injected with 240 MBq of FDG had a double set of emission scans (8-64 sec in 2D and 8-512 sec in 3D) of the brain starting 2 hours after injection, followed by a double set of transmission scans (32-512 sec) yielding a total of 35 data points in (E,T). Reconstruction and data analysis matched the brain phantom F-18 series.

One patient (case BB) undergoing a dynamic FDG scanning of the heart additionally had a series of transmission scans, (0.5,1,2,4,8,20) minutes. Pairs of emission scans (0.5,1,2,5 minutes) from different parts of the dynamic study were reconstructed with all the transmission scans with subsequent data analysis in a large body circumferential ROI.

IV. Results

In this section data and parameters are presented for the previously described experiments and compared to the model.

A. *The Cylinder and Elliptical Body phantom*

Estimated parameters for the Cylinder phantom in 2D and 3D modes, and the Elliptical Body phantom in 2D and 3D are given in table 1 and 2.

Table 1: Cylinder data 2D and 3D

	Cylinder 2D	Cylinder 3D
a [M Counts]	4.77E-2	2.70E-2
b [ ]	1.88E-3	3.49E-4
c [sec]	6.40	1.64
d [sec]	0.96	
Min(NEC) [M-Counts]	0.43	1.48
Max(NEC) [M-Counts]	13.00	38.75
Min(T_t) [sec]	64	256
Max(T_t) [sec]	32768	32768
Min($\frac{V}{E^2}$)	5.60E-3	1.10E-3
Max($\frac{V}{E^2}$)	1.60E-1	2.46E-2
Max(Error)	1.26E-4	3.02E-6

Table 2: Elliptical body phantom data 2D and 3D

	Ellipse 2D	Ellipse 3D
a [M Counts]	2.46E-2	3.38E-2
b [ ]	1.67E-3	1.54E-3
c [sec]	8.85	4.16
Min(NEC) [M-Counts]	0.17	2.50
Max(NEC) [M-Counts]	9.60	27.83
Min(T_t) [sec]	1024	1024
Max(T_t) [sec]	16384	32768
Min($\frac{V}{E^2}$)	4.01E-3	2.79E-3
Max($\frac{V}{E^2}$)	1.56E-1	1.94E-2
Max(Error)	4.77E-5	9.40E-6

In the following two Figures of the normalized variance are shown as a function of NEC and transmission scan length T_t. Figure 1 corresponds to the Cylinder (2D) and Figure 2 to the Cylinder (3D).

Also in the Brain phantom (3D) case and in case MN both the emission and transmission parameters have been estimated. The parameters are listed in Table 3 together with the range of the fit. Figure 3 shows the normalized variance for the Brain phantom and Figure 4 demonstrates that the model fits the measured data nicely.

To illustrate how well the emission data measured on brains agree with the phantom studies, Figure 5 shows case KL (2D/3D), case MN (2D/3D), and the Brain Phantom (2D/3D). In all cases data corresponding to only one transmission scan are shown.

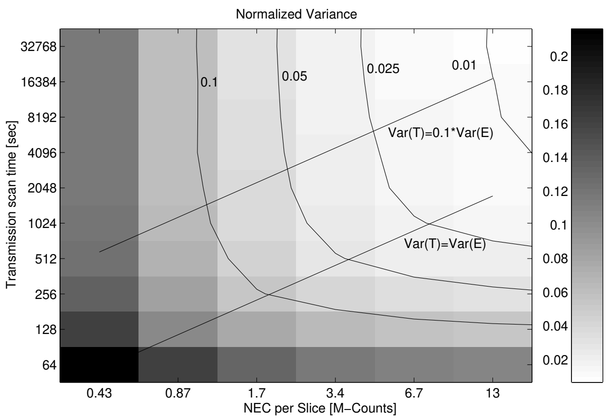

Figure 1: Normalized variance of Cylinder (2D) as a function of NEC per slice and duration of transmission scan T_t. Contours show iso-noise curves with levels indicated. Lines show where the ratio of transmission to emission noise terms is unity and 10% respectively.

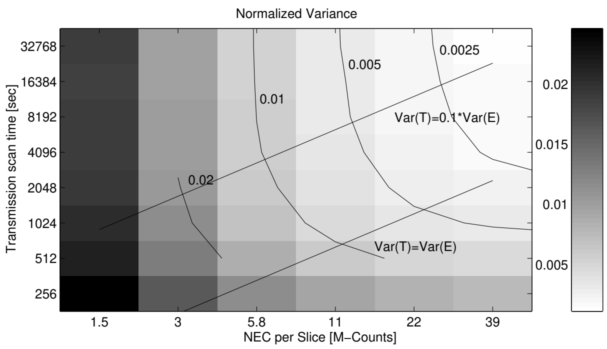

Figure 2: Normalized variance Cylinder (3D) as a function of NEC per slice and duration of transmission scan T_t..

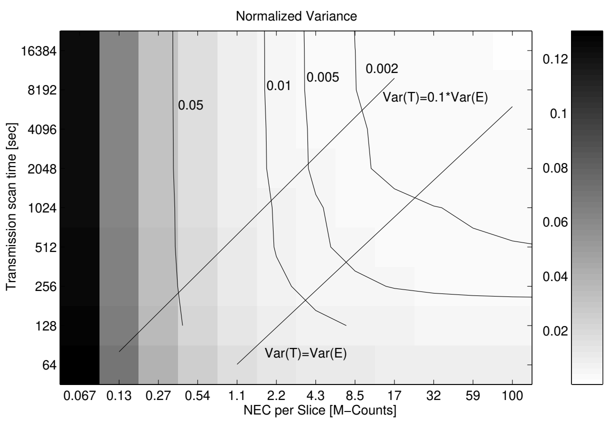

Figure 3: Normalized variance of Brain phantom (3D) as a function of NEC per slice and duration of transmission scan T_t.

Table 3: Brain phantom data 3D and Case MN 3D

	Brain Ph.	Case MN
a [M Counts]	1.67E-2	1.85E-2
c [sec]	1.01	1.59
Min(NEC) [M-Counts]	6.7E-2	6.4E-1
Max(NEC) [M-Counts]	2.2	3.6
Min(T_t) [sec]	64	64
Max(T_t) [sec]	16384	512

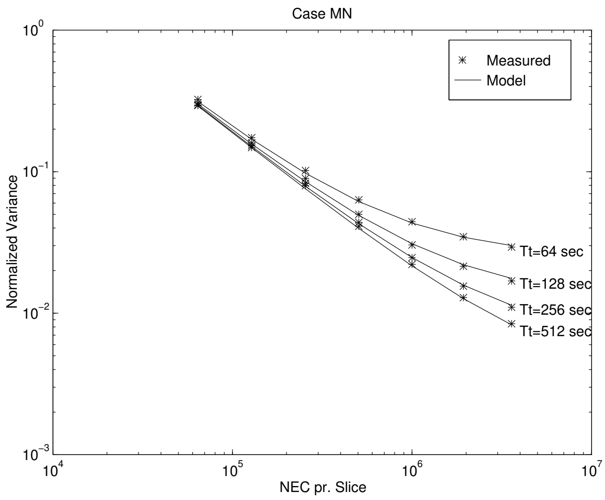

Figure 4: Normalized variance of case MN (3D) as a function of NEC per slice and duration of transmission scan T_t. Stars show the measured data and lines the fitted model.

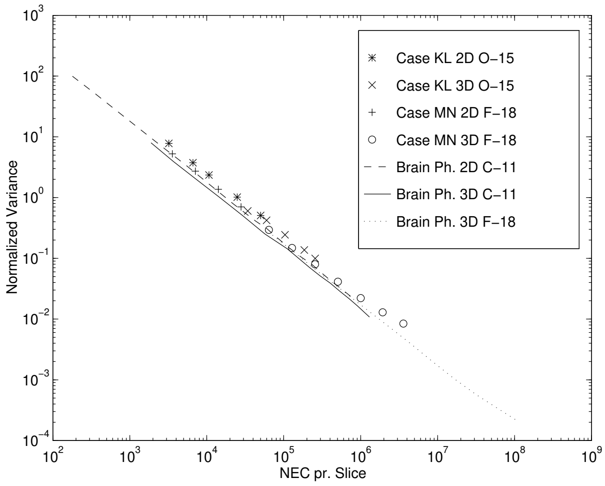

Figure 5: Normalized variance of Case KL (2D/3D), case MN (2D/3D), and Brain phantom (2D/3D) as a function of NEC per slice.

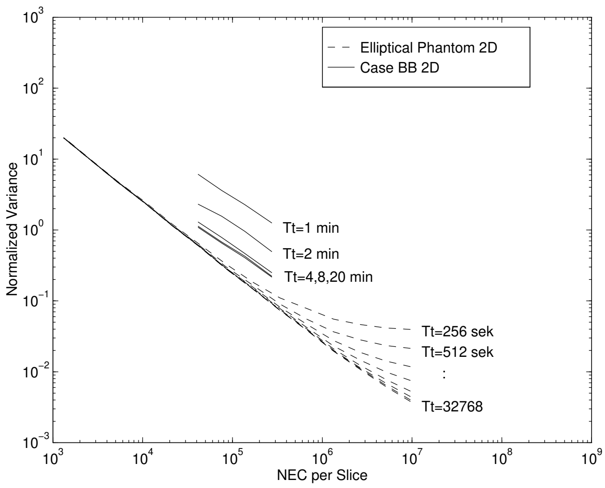

Figure 6: Normalized variance of body studies case BB (2D) and Elliptical phantom (2D) as a function of NEC per slice. Note that case BB (1,2 and 4 min) shows a different noise behavior.

Figure 6 shows body data. The 2D Elliptical Body phantom follows the previous noise model, but in case BB (large patient with arms in FOV) the noise curves for the 1 and 2 minutes transmission scans are shifted upwards. Inspection of the reconstructed images reveals large number of lines, due to (clusters of) zeros in the transmission scan.

V. Discussion

The general noise properties of reconstructive tomography are well described in the literature [1, 2]. Previous descriptions of the Advance scanner also include count rate dependence in phantoms and humans [8, 4] but the noise characterization so far [5] focused on the emission noise. In this paper we have determined the relative importance of the noise contributions from blank, transmission, and emission scans for a range of imaging situations encountered.

As shown, a good fit to the empirical variance is found both in 2D and 3D studies. The numerical values of the measure chosen for the noise examination is strongly dependent on reconstruction parameters, in part because of the neighbor pixel correlation disregarded in the theory section. Most parameters, however, will affect the Emission and Transmission contributions in the same way (through ϕ_{ij} only), and therefore the model and its output is considered adequate for the purpose of identifying areas in the E-T plane where one source is dominating.

From Table 1 it is seen that the blank scan contribution to the noise as expected is only a small fraction of the transmission for same duration, the ratio being well explained by the average attenuation of the (central part of) the 20 cm Cylinder phantom. For all practical purposes, therefore, the application of a 20 minutes blank scan will ensure that the blank scan contribution is negligible since the cases where a longer transmission scan might be applied are those with a higher attenuation.

A typical 3D brain activation study with O-15 water in our setup will contain 0.5 Mcounts/central slice, Figure 5,[4]. With a 10 minutes transmission scan, the transmission variance calculated from the phantom data in Table 3 is 1.67E-3 compared to the emission contribution of 3.34E-2, i.e., the transmission adds (only) 5% to the final result. For the human case MN the corresponding figures would be 2.65E-3 (transmission), 3.7E-2 (emission) and 7%, respectively. A 10 minutes, 2D FDG brain scan typically would also have 0.5-1 M counts yielding the same 5-10% ratio, while acquiring the same data in 3D would make the two contributions almost equal and therefore call for a more detailed analysis. It should be noted that in this imaging condition no attribute has been made to the additional noise from the emission correction of the transmission scan which is necessary if the transmission is performed with activity present.

Figure 6 suggests that within the emission count range of a typical dynamic heart FDG scan, the transmission noise contribution (from a 20 minutes transmission scan) is not dominating. Data are, however, not available that can demonstrate the region in which the transmission noise curves split up. It should be emphasized that the observed shift of the short-time curves is due to line-artefacts caused by (clusters of) zeros in the transmission sinogram. This deteriorating effect is usually more important and calls for improved method of attenuation correction, e.g., by using image segmentation as described in [7].

References

[1] A. E. Todd-Pokropek and P. H. Jarrit. The noise characteristics of SPECT systems. In P. J. Ell and B. L. Holman, editor, *Computed Emission Tomography*, pages 361–389. Oxford University Press, Oxford, 1982.

[2] N. M. Alpert et al. Estimation of the Local Statistical Noise in Emission Computed Tomography. *IEEE Trans. Med. Imag.*, MI-1(2):142–146, 1982.

[3] S. C. Strother et al. Measuring PET Scanner Sensitivity: Relating Count Rates to Image Signal-to-Noise Ratios Using Noise Equivalent Counts. *IEEE Trans. Nucl. Sci.*, NS-37(2):783–788, April 1990.

[4] S. Holm et al. 3D PET activation studies with $H_2{}^{15}O$ bolus injection. Count rate performance and dose optimization. In *Quantification of Brain Function using PET*. Academic Press, San Diego, 1995. In press.

[5] S. Pajavic et al. Noise Properties of 3D PET Images. *J. Nucl. Med.*, 36:p. 105 (abstract), 1995.

[6] S. R. Cherry et al. Improved Detection of Focal Cerebral Blood Flow Changes Using Three-Dimensional Positron Emission Tomography. *J. Cereb Blood Flow Metab*, (4):630–638, 1993.

[7] S. R. Meikle et al. Attenuation Correction Using Count-Limited Transmission Data in Positron Emission Tomography. *J. Nucl. Med.*, 34:143–150, 1993.

[8] T. K. Lewellen et al. Investigations of the Count Rate Performance of General Electric Advance Positron Emission Tomograph. *IEEE Trans. Nucl. Sci.*, NS-42(4):1051–1057, August 1995.

[9] T. R. DeGrado et al. Performance Characteristics of a Whole-Body PET Scanner. *J. Nucl. Med.*, 35(8):1398–1406, 1994.